Proceedings of the 28th IEEE
EMBS Annual International Conference
New York City, USA, Aug 30-Sept 3, 2006

Gradient Distortion Correction for Low Frequency Current Density Imaging

Charles X. B. Yan, Tim P. DeMonte, *Member*, IEEE, Michael L. G. Joy, *Member*, IEEE

***Abstract*—Current density imaging (CDI) is a technique that uses magnetic resonance imaging (MRI) to measure the distribution of externally applied electric current inside tissues. However, CDI processing is rendered inaccurate by the distortion caused by the nonlinearity of MRI gradient fields. The distortion interferes with the proper registration and the curl operation required for correct computation of current density vectors. To address this problem, a calibration phantom was imaged to determine the distortion and to generate calibration maps to correct the distorted current density images. A validation experiment involving a cylindrical phantom was performed to verify this method. Comparison of the distorted and corrected images reveals that both the registration and the curl operation are successfully corrected by this method.**

I. Introduction

Current density imaging (CDI) is a technique that uses magnetic resonance imaging (MRI) to measure the distribution of externally applied electric current inside conductive media, including biological tissues. One important application of CDI is to study current pathways through the heart and chest of postmortem pigs to improve defibrillator design [1]. Currently, the most mature CDI technique is low frequency CDI (LFCDI). Throughout this paper, the term CDI is used to refer to the LFCDI technique. CDI relies on the spatial localization capability of the MRI and one of Maxwell's quasi-static equations as in

$$\mathbf{J} = \frac{1}{\mu_0}\nabla \times \mathbf{B} = \frac{1}{\mu_0}\left[\left(\frac{\partial B_z}{\partial y} - \frac{\partial B_y}{\partial z}\right)\hat{i} + \left(\frac{\partial B_x}{\partial z} - \frac{\partial B_z}{\partial x}\right)\hat{j} + \left(\frac{\partial B_y}{\partial x} - \frac{\partial B_x}{\partial y}\right)\hat{k}\right] \quad (1)$$

The current density vector **J** is computed from the curl of the magnetic field vector **B** [2]. The magnetic field **B** is measured by the MRI, encoded in the phase images, and is directly proportional to the encoded phase value. Therefore, in the actual implementation, CDI computes current density vectors from the encoded phase information. The curl operation requires knowledge of magnetic field components in three orthogonal directions. CDI obtains the three components separately in three imaging sessions. For this reason, the images representing these three components need to be properly registered to correctly compute the current density vector **J**. However, gradient distortion artifacts caused by MRI hardware limitations prevent proper registration and distort the spatial derivatives within the curl operation, making computation of the current density inaccurate. This paper investigates the possibility to measure and to correct the gradient distortion in CDI.

A. Distortion due to Gradient Field Nonlinearity

In MRI, image object signals are spatially localized by the use of gradient magnetic fields. The gradient fields encode the position of the signals by frequency encoding or phase encoding as

$$\omega(x) = \omega_0 + \gamma x G_x \quad (2)$$

$$\phi(x) = -\gamma x G_x T_{pe} \quad (3)$$

where $\omega(x)$ is the precessing frequency, ω_0 is the Larmor frequency, γ is the gyromagnetic ratio, G_x is a linear gradient field, $\varphi(x)$ is the phase angle, and T_{pe} is the phase encoding time interval [3]. Equation (2) is one-dimensional frequency encoding and equation (3) is one-dimensional phase encoding. Although both equations only demonstrate encoding in the *x* direction, they are equally applicable in the *y* and *z* directions. Note that in both cases, the precessing frequency or phase angle are linearly proportional to the position *x* of the signal. If the gradient field becomes nonlinear, then an additional nonlinear term $G'(x,y,z)$ will be added to G_x, and the equations become

$$\begin{aligned}\omega(x) &= \omega_0 + \gamma x\left(G_x + G'(x,y,z)\right) \\ &= \omega_0 + \gamma x G_x\left(1 + \frac{G'(x,y,z)}{G_x}\right) \\ &= \omega_0 + \gamma x' G_x \end{aligned} \quad (4)$$

$$\begin{aligned}\phi(x) &= -\gamma x\left(G_x + G'(x,y,z)\right)T_{pe} \\ &= -\gamma x G_x\left(1 + \frac{G'(x,y,z)}{G_x}\right)T_{pe} \\ &= -\gamma x' G_x T_{pe} \end{aligned} \quad (5)$$

Manuscript received July 11, 2006. This work was supported in part by Philips Medical Systems (Seattle, USA defibrillation research group) and Natural Sciences and Engineering Research Council of Canada (NSERC).

C. X. B. Yan is with the Institute of Biomaterials and Biomedical Engineering, University of Toronto, Toronto, ON M5S 3G9 Canada (e-mail: charles.yan@utoronto.ca).

T. P. DeMonte is with Field Metrica Inc., Toronto, ON M8V 1W1 Canada (phone: 416-259-9842; e-mail: tdemonte@fieldmetrica.com).

M. L. G. Joy is with the Institute of Biomaterials and Biomedical Engineering, University of Toronto, Toronto, ON M5S 3G9 Canada (e-mail: mikejoy@ecf.utoronto.ca).

where the distorted position $x' = x\left(1 + \frac{G'(x,y,z)}{G_x}\right)$ will be the actual position encoded. In this way, the image object signal located at position x is spatially distorted to position *x*' [4]. Note that spatial distortion is not the only distortion caused by gradient nonlinearity. The intensity of the magnitude image is also distorted due to distortion in the sampling volume elements. More details on the theory of intensity distortion can be found in [5].

B. Effects of Gradient Distortion on CDI

Gradient distortion causes current density computation to be inaccurate for two main reasons: mis-registration of magnetic field components and taking phase derivatives with respect to the distorted coordinate system. Mis-registration is caused by the asymmetry of spatial distortion in the three orthogonal directions in which the magnetic field components are acquired. Due of this asymmetry, image voxels that would otherwise be registered together undergo different distortion displacements and are broken apart from each other. Mis-registration causes signals measured from different volume elements to be combined, and the current density **J** in turn is computed from unrelated magnetic field components, resulting in erroneous value. In equation (1), the curl operation involves taking derivatives of magnetic field components. Since the magnetic field is proportional to the phase value encoded, taking spatial derivative of magnetic field components is equivalent to taking the derivative of phase components. However, due to spatial distortion, the coordinate system in which the spatial derivative is computed is distorted. The resulting current density vector points to a direction in the distorted space.

Previous works studied the effects of mis-registration that gradient distortion had on CDI [6], [7]. In addition to the mis-registration problem, this paper also takes into account the distortion experienced by the phase derivatives. A full CDI distortion correction is performed by correcting both the spatial distortion and the phase derivative distortion.

II. METHODOLOGY

A calibration phantom was used to measure the distortion caused by the nonlinearity of gradient fields. The phantom consists of a 3D grid of acrylic spheres. The spheres are 8 mm in diameter and are regularly spaced 15 mm center-to-center, as shown in Fig. 1. There are 13,716 spheres in total and the size of the phantom nearly fills the entire magnetic bore of the MRI scanner used. The large size of the phantom ensures maximum coverage of distorted area in the image field of view (FOV). Before the phantom is imaged, the spheres are filled with deionized water that produces magnetic resonance (MR) signals. Because acrylic material does not produce MR signals, the resulting magnitude image of the phantom only contains signals from the water-filled spheres.

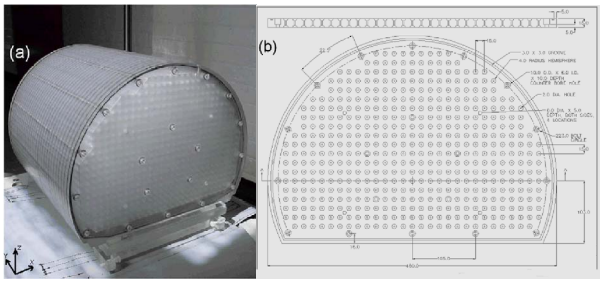

Fig. 1. The calibration phantom consists of a 3D grid of acrylic spheres with 8 mm diameter and regularly spaced 15 mm center-to center. (a) Photograph and (b) CAD drawing.

Due to gradient distortion, the spheres in the image are no longer at their expected position, as shown in Fig. 2a. From the figure, it can be observed that the nonlinearity of the gradient fields is such that there is no distortion at the isocenter of the FOV, and high distortion at the four corners. To extract the distortion pattern from the phantom image, an image processing algorithm first detects the position of each sphere in the distorted image. It then matches the distorted position of the spheres to their expected position in an ideal undistorted image. The undistorted position of the spheres can be computed because the physical design parameters of the phantom are already known beforehand. In this way, the matching of the distorted position to the undistorted position creates a calibration map that contains the distortion pattern. Application of the calibration map on the distorted image results in the corrected image shown in Fig. 2b.

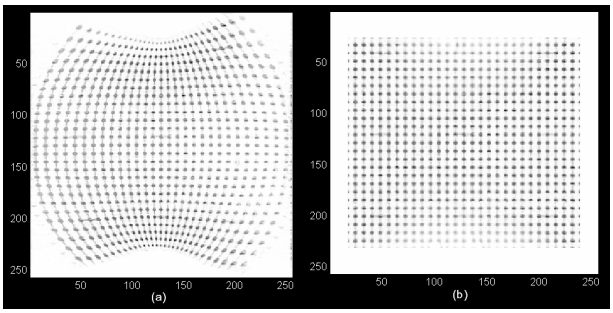

Fig. 2. (a) The distorted calibration phantom magnitude image shows that the spheres are displaced away from their expected position in the regular 3D grid. There is no distortion at the isocenter and high distortion at the four corners. (b) The corrected magnitude image of the phantom shows the expected regular grid of spheres.

The direct application of the calibration map can correct the spatial distortion by bringing any data point from its distorted position to its undistorted position. However, as pointed out previously, spatial distortion only solves the problem of mis-registration. The fact that the phase derivatives are taken with respect to the distorted coordinate system also needs to be addressed. To transform the derivatives from the distorted coordinate system to the undistorted one, the Jacobian matrix of the calibration map is multiplied to the components of the vector as

$$\frac{d\phi}{dx} = \frac{\partial\phi}{\partial u}\frac{\partial u}{\partial x} + \frac{\partial\phi}{\partial v}\frac{\partial v}{\partial x} + \frac{\partial\phi}{\partial w}\frac{\partial w}{\partial x}$$
$$\frac{d\phi}{dy} = \frac{\partial\phi}{\partial u}\frac{\partial u}{\partial y} + \frac{\partial\phi}{\partial v}\frac{\partial v}{\partial y} + \frac{\partial\phi}{\partial w}\frac{\partial w}{\partial y} \quad (6)$$
$$\frac{d\phi}{dz} = \frac{\partial\phi}{\partial u}\frac{\partial u}{\partial z} + \frac{\partial\phi}{\partial v}\frac{\partial v}{\partial z} + \frac{\partial\phi}{\partial w}\frac{\partial w}{\partial z}$$

where φ is the phase, (x,y,z) is the coordinate system in the undistorted space, and (u,v,w) is the coordinate system in the distorted space. The calibration map can be considered as functions that express (u,v,w) in terms of (x,y,z).

A validation experiment was performed to evaluate the effectiveness of the gradient distortion correction method by using the calibration maps generated. The experiment uses a cylinder shaped phantom, in which the bases are two copper plate electrodes. Externally applied electric current is injected through the top electrode and leaves at the bottom one. Before imaging, the phantom is filled with water containing $CuSO_4$ and NaCl for better MR signal and better current conductivity respectively. Fig. 3 shows the water-filled phantom just before the experiment. Due to the symmetry of the phantom, it is expected that current will flow coherently only along the longitudinal direction of the cylinder. During the validation experiment, the phantom is placed at lower right corner of the calibration phantom's FOV, where the gradient distortion is highest (see Fig. 2a). In this way, the resulting current density image will face the most severe mis-registration and derivative problems caused by gradient distortion.

Fig. 3. A cylinder shaped phantom in which the bases are two copper plate electrodes. The cylinder is filled with water containing $CuSO_4$ and NaCl. Externally applied current is injected through the top electrode and leaves at the bottom one.

III. Results

The results of the validation experiment are shown in Fig. 4 and Fig. 5. Fig. 4 shows the magnitude and current density data without any correction. The data in Fig. 5 have been corrected using the calibration map generated from the calibration phantom. In both figures, the magnitude image has been rendered in 3D using isosurface, and opacity set to 50% to allow the streamlines inside the phantom to be seen. The two groups of streamlines in each figure are generated from seed points with the same coordinates, one in the middle and one near the right side of the cylinder. The streamlines enable easier visualization of current flow at the two areas of interest. In addition, in Fig. 5, a noise-masked portion of the current density vector data was overlaid on the isosurface. The small black arrows represent current density vectors in a plane near the center of the cylindrical phantom.

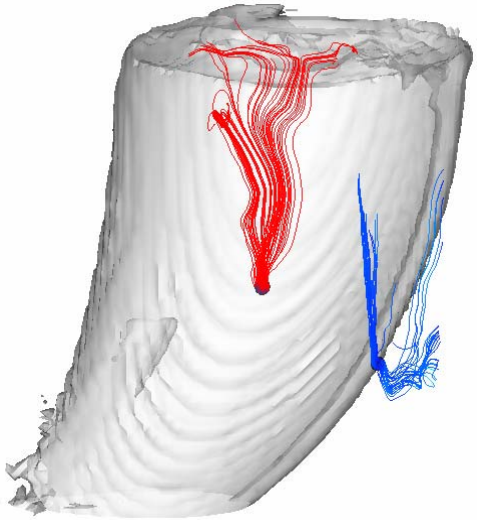

Fig. 4. A 3D rendering of the distorted image. The shape of the phantom image is displayed using isosurface with opacity set to 50%. The group of streamlines in the middle (red) shows divergent current flow due to distorted phase derivatives. The group of streamlines on the right (blue) shows random current density vectors due to mis-registration of magnetic field components.

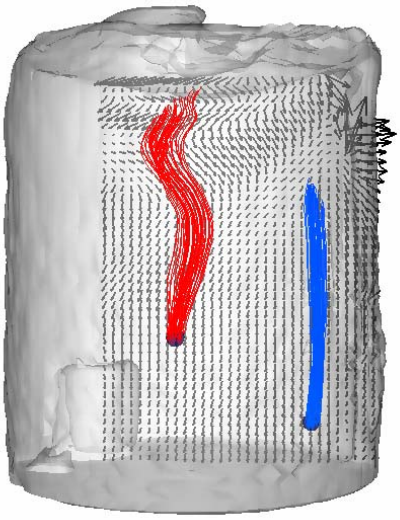

Fig. 5. A 3D rendering of the corrected image. The shape of the phantom image is displayed using isosurface with opacity set to 50%. Both the middle (red) and right (blue) groups of streamlines form narrow bands indicating uniform current flow. The group of streamlines on the right shows the expected longitudinal current flow.

IV. Discussion

Comparison of the distorted image in Fig. 4 and the corrected image in Fig. 5 clearly shows that distortion correction is successful for the magnitude image of the cylindrical phantom. The position of the phantom in the FOV is such that the distortion is highest near the bottom of the cylinder, where there are large displacements towards the left. These displacements have been corrected in the undistorted space as shown in Fig. 5.

Comparison of the streamlines also shows significant correction in current density vectors. The group of streamlines on the right near the edge of the cylinder (shown in blue) traces current flowing in the longitudinal direction. In the distorted image, although some streamlines trace some coherent current flow, a significant number of others go astray and behave in a random fashion. By making reference to the isosurface, it can be seen that the seed point of this group of streamlines falls on the edge of the distorted cylinder. Consequently, the neighboring current density vectors on the other side of the distorted edge are computed from distorted magnetic field components mis-registered with noise, even if they are still within the boundaries of the actual phantom. On the other hand, in the corrected image, the group of streamlines generated from the same seed point forms a narrow band and traces a straight longitudinal current flow as in the expected result, demonstrating that mis-registration is resolved in the corrected image.

The group of streamlines generated by the seed point in the middle (shown in red) has been configured to trace all the way back to the copper plate electrode where current is injected. The streamlines in the distorted image start to diverge as soon as they leave the seed point and end up far from each other on the electrode. This type of behavior is partly attributed to mis-registration but more importantly, to the distorted spatial derivatives, because the direction of the current flow is determined by the relative strength of each component in the current density vector and the components are in turn computed from derivatives taken with respect to the distorted coordinate system. As a result, the current density vectors are directed in the distorted space. However, in the corrected image, the streamlines stay relatively parallel to each other and keep the band shaped grouping until they reach the electrode, indicating successful correction of the distorted derivatives. Therefore, both groups of streamlines demonstrate improvements in the accuracy of current density computation in the corrected image.

The validation of gradient distortion correction has been qualitative until now. Further analysis is required to confirm the effectiveness of the current method. Possible quantifiable validations are the computation of signal to noise (SNR) ratio of the uniform current density vectors and the comparison of the current density integration with the total current injected.

It is worth mentioning that some commercial scanner manufacturers provide their own gradient distortion correction software for the magnitude images. However, gradient distortion artifacts in CDI cannot be effectively corrected by these softwares for several reasons. Firstly, some people have found the manufacturers' correction algorithm based on the theoretical design parameters to be inaccurate, because even gradient coils made from the same design could have winding errors, causing variations from the predicted field [8]. In the second place, the manufacturers' softwares cannot directly correct phase images because of the existence of phase wraps. To enable phase correction using these softwares, 3D phase unwrapping algorithms would have to be employed, which are less efficient and less reliable than the 1D phase unwrapping algorithm currently used by CDI processing. Finally, it is also impractical to seek the gradient coil design parameters from the manufacturers for correction purposes, because they usually do not release these commercially sensitive information.

V. Conclusion

The gradient distortion correction method presented in this paper has been demonstrated to successfully correct the mis-registration and derivative distortion problems associated with distorted current density images.

Acknowledgment

C. X. B. Yan would like to thank Weijing Ma and Dinghui Wang for their insightful ideas during this project.

References

[1] R. S. Yoon, T. P. DeMonte, K. F. Hasanov, D. B. Jorgenson, and M. L. G. Joy. "Measurement of thoracic current flow in pigs for the study of defibrillation and cardioversion," *IEEE Trans. Biomed. Eng.*, Vol. 50, No. 10, pp. 1167-1173, Oct. 2003.

[2] G. C. Scott, M. L. G. Joy, R. L. Armstrong, and R. M. Henkelman. "Measurement of nonuniform current density by magnetic resonance," *IEEE Transactions on Medical Imaging*, Vol. 10, No. 3, pp. 362-374, 1991.

[3] Z. P. Liang and P. C. Lauterbur, *Principles of Magnetic Resonance Imaging: A Signal Processing Perspective*, Piscataway, N.J.: IEEE Press Series in Biomedical Engineering, 2000, ch. 5.

[4] E. M. Haacke, R. W. Brown, M. R. Thompson, and R. Venkatesan, *Magnetic Resonance Imaging: Physical Principles and Sequence Design*, New York, N.Y.: Wiley-Liss, 1999, ch. 20.

[5] H. Chang and M. Fitzpatrick. "A technique for accurate magnetic resonance imaging in the presence of field inhomogeneities," *IEEE Transactions on Medical Imaging*, Vol. 11, No. 3, pp. 319-329, Sept. 1992.

[6] T. P. DeMonte, R. S. Yoon, K. F. Hasanov, D. B. Jorgenson, and M. L. G. Joy. "Image distortion and image mis-registration in low frequency current density imaging," presented at the *24th Ann. Int. Conf. IEEE EMBS*, Houston, Texas, USA, pp. 933-934, 2002

[7] T. P. DeMonte, R. S. Yoon, D. B. Jorgenson, and M. L. G. Joy. "Effects of gradient distortion on low frequency current density imaging," presented at *ISMRM, XI'th Sci. Meet. and Exh.*, Toronto, Canada, 2003

[8] A. Janke, H. Zhao, G. J. Cowin, G. J. Galloway, and D. M. Doddrell. "Use of spherical harmonic deconvolution methods to compensate for nonlinear gradient effects on MRI images," *Magnetic Resonance in Medicine*, Vol. 52, pp. 115-122, July 2004.